An adaptive-remeshing framework to predict impact-induced skull fracture in infants

Junyan He, Jiawei Yan, Susan Margulies, Brittany Coats & Ashley D. Spear

Biomechanics and Modeling in Mechanobiology

ISSN 1617-7959

Biomech Model Mechanobiol
DOI 10.1007/s10237-020-01293-9

Springer

Biomechanics and Modeling in Mechanobiology
https://doi.org/10.1007/s10237-020-01293-9

ORIGINAL PAPER

An adaptive-remeshing framework to predict impact-induced skull fracture in infants

Junyan He[1] · Jiawei Yan[1] · Susan Margulies[2] · Brittany Coats[1] · Ashley D. Spear[1]

Received: 24 September 2019 / Accepted: 14 January 2020

Abstract
Infant skull fractures are common in both accidental and abusive head trauma, but identifying the cause of injury may be challenging without adequate evidence. To better understand the mechanics of infant skull fracture and identify environmental variables that lead to certain skull fracture patterns, we developed an innovative computational framework that utilizes linear elastic fracture mechanics theory to predict skull fracture as a first step to study this problem. The finite element method and adaptive-remeshing technique were employed to simulate high-fidelity, geometrically explicit crack propagation in an infant skull following impact. In the framework, three modes of stress intensity factors are calculated by means of the *M*-integral using the commercial analysis code, FRANC3D, and are used as measures of crack driving force. The anisotropy of infant skulls is represented by means of a transversely isotropic constitutive model and a direction-dependent fracture-toughness locus. The ability of the framework to predict impact-induced fracture patterns is validated by comparison with experimentally observed fracture patterns from the literature.

Keywords Computational fracture mechanics · Infant skull fracture · Crack growth · Linear elastic fracture mechanics

1 Introduction

In 2017, approximately 3.5 million children in the USA were victims of child maltreatment and abuse (USDHHS 2019). Under current Department of Justice guidelines, an important indicator of physical abuse is the inability of the caretaker to provide a history that corresponds to the observed injuries of the child (Farley et al. 2002). When no history of trauma is presented, identifying discrepancies to injuries may be straightforward. However, when a history of a fall is provided, distinguishing between abusive and accidental trauma proves to be challenging, especially if the injuries are limited to skull fracture and underlying head trauma. Skull fractures are common in both accidental and abusive head trauma (Leventhal et al. 1993), but very little is known about the mechanics of skull fractures from accidental falls in infants. The ability to objectively identify the cause of skull fracture and understand the sensitivity of skull fracture patterns to impact conditions (i.e., direction, height, surface conditions) can substantially improve the accurate detection of child abuse.

Previous experimental research efforts have focused on exploring the impact response of the infant head and the connections between types of loading and the resulting skull fracture patterns (Weber 1984, 1985; Loyd 2011). In these three studies, cadavers were dropped from various heights onto various surfaces. Unfortunately, detailed quantitative descriptions of the impact conditions are lacking in many of the studies. In the most recent study, Loyd (2011) studied the force and acceleration curves from infant cadaver head drop experiments and reported skull fracture patterns. Compared to the work by Weber (1984, 1985), Loyd (2011) provided more information on the head orientation prior to each drop, but the exact impact location and impact angle were not measured. These limitations make computational modeling challenging, but the studies still provide valuable data to qualitatively validate skull fracture predictions.

Realizing the lack of sufficient human specimens to perform comprehensive tests, researchers have explored pediatric head injury from a computational perspective. Finite element (FE) models have been constructed from computed

✉ Ashley D. Spear
ashley.spear@utah.edu

[1] Department of Mechanical Engineering, University of Utah, Salt Lake City, UT, USA

[2] Department of Biomedical Engineering, Georgia Institute of Technology and Emory University, Atlanta, GA, USA

Published online: 27 January 2020

tomography (CT) scans and used to simulate the stress and strain response of the human infant skull during impact (Li et al. 2013, 2015). Comparing the stress/strain fields from FE simulations and the observed fracture patterns, researchers have formulated crack-initiation criteria that identify potential initiation sites for cracks (Coats et al. 2007; Coats 2007; Roth et al. 2008; Hajiaghamemar et al. 2018). These studies use high-strain-rate material property data from infant skull specimens (Coats and Margulies 2006), but none of the above-mentioned works explore how cracks propagate under the given loads. More recent studies investigated crack propagation in infant skulls using an element deletion method (Zhang et al. 2001; Lee et al. 2009; Sahoo et al. 2013; Asgharpour et al. 2014). Element deletion is a commonly used method because it requires minimal modification to the standard FE procedure. In this method, a damage variable is calculated based on a damage criterion, and stress is scaled down based on this damage variable. When an element fails, its stress is reduced to zero. By sequential failure of elements, a "crack" can be formed and propagated. Because elements of the mesh are deleted, the final fracture patterns depend on the initial mesh. Furthermore, no crack geometry is included in this method; therefore, the singular stress/strain fields near the crack tip that dictate the crack path are not captured. In other words, the deletion of elements simply leads to the appearance of a fracture surface, but fracture is technically not simulated. Other computational methods like the extended finite element method (Song et al. 2006) and adaptive remeshing (Davis et al. 2014) have been used to study crack propagation in complex geometries. However, the application of such methods has been mostly focused on analyzing engineering components and structures, not biological structures. The area of studying crack propagation on biomaterials using well-established computational fracture mechanics methods remains largely unexplored.

The objective of this work was to develop a sophisticated computational framework that can assist in the differential diagnosis between accidental and abusive head trauma by enabling high-fidelity simulation of crack propagation in infant skulls using principles of linear elastic fracture mechanics (LEFM). To achieve this objective, we selected an adaptive-remeshing technique to predict crack propagation. In this method, the crack face is first represented as a virtual boundary in the geometry. Every time the crack propagates, the mesh is updated and the element edges and faces are forced to conform to this virtual boundary. In this way, the crack face is represented explicitly in the resulting mesh by element edges and faces. To capture the high-gradient stress field, quarter-point elements can be used, which produce the desired singularity in the element shape functions (Shih et al. 1976; Lynn and Ingraffea 1978). Various examples of adaptive remeshing can be found in the literature (Wawrzynek et al. 2010; Chin 2011; Spear et al. 2011; Davis et al. 2014). The largest disadvantage of this method is the constant need to remesh. However, adaptive remeshing is more appropriate when dealing with crack-face contact (Corbani et al. 2018) as well as crack closure (Nguyen et al. 2001). In addition, because quarter-point elements are used near the crack tip, a relatively coarse mesh can still provide an accurate characterization of the stress field. Finally, among all of the available FE-based approaches, adaptive remeshing can conform to complex, three-dimensional crack surfaces as predicted by fracture mechanics, thus resulting in minimal mesh dependency. Once developed, this novel computational framework will be invaluable to the investigation of skull fracture patterns in infants from accidental and abusive head trauma.

2 Framework development

2.1 Overview of framework

The overarching goal of this framework is to simulate crack propagation in an infant skull FE model. To do so, we start by inspecting the stress/strain distribution throughout an uncracked model during a simulated impact event to identify potential locations of crack initiation, similar to our previous work (Coats et al. 2007; Hajiaghamemar et al. 2018). Once the location of crack initiation is determined, we identify the preferred crack orientation by comparing stress intensity factors (SIFs) for cracks inserted at the same location but with different orientations. When both the location and orientation are determined, we employ the commercial software FRANC3D (Wawrzynek et al. 2010) to insert the initial crack. We discretize the crack-growth process into crack-growth time steps. In each time step, SIFs are computed and used to determine whether the crack will propagate, and if so, in what direction. Every time a crack is propagated, crack stability is checked, and the crack is propagated in the same time step if it is unstable. A high-level flowchart of the simulation framework is provided in Fig. 1. The following subsections describe each step in detail.

2.2 Model definitions

An impact case is uniquely defined by the skull geometry, material properties, impact direction, and impact height. The skull FE model used in this work is adopted from the work by Coats et al. (2007). The material properties used in the model are presented in Table 1, and are adopted from works by Metcalf et al. (2019), Coats and Margulies (2006) and Peterson and Dechow (2002).

To account for the trabecular fibers growing outward from the ossification centers of the infant skull (Cunningham et al. 2016), three cylindrical coordinate systems were

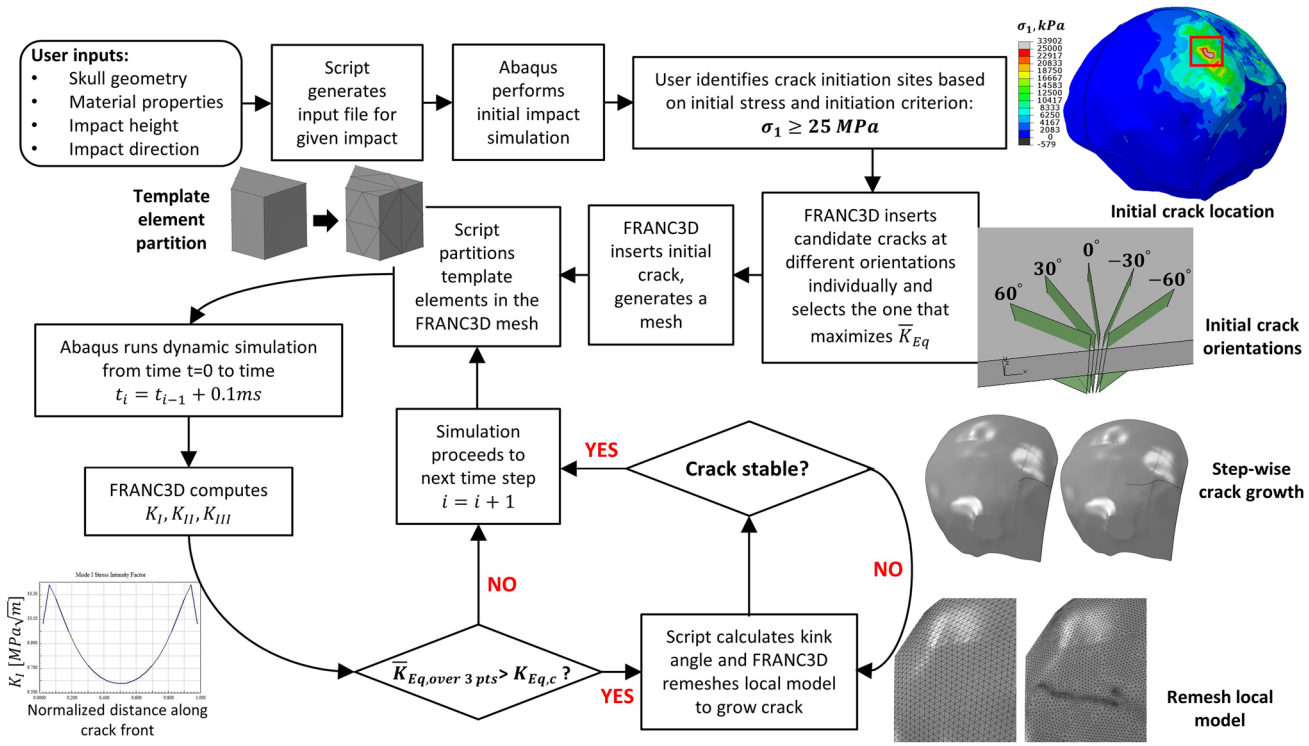

Fig. 1 Adaptive-remeshing framework for simulating crack growth during an explicit dynamic simulation

Table 1 Material properties of the infant skull FE model in this work

Region	E_1 (MPa)	E_2 (MPa)	E_3 (MPa)	ν_{12}	ν_{23}
Parietal	4677	453	453	0.28	0.465
Occipital	4022	300	300	0.28	0.465
Rest of skull	407	407	407	0.19	0.19
Suture	8.1	8.1	8.1	0.49	0.49

established to define the local material orientation on the left parietal bone, right parietal bone, and occipital bone, respectively. The origin of each coordinate system is located at the ossification center of each cranial bone. An example of the cylindrical coordinate system is depicted in Fig. 2 on the right parietal bone of the FE model. The moduli, E_1, E_2, and E_3, are along the principal material axes, e_1, e_2, and e_3, where e_1 and e_2 are aligned with radial and tangential directions, respectively, and e_3 is orthogonal to e_1 and e_2. Because this work only focuses on crack propagation in the parietal and occipital regions of the skull, only those regions were assigned anisotropic material properties. The rest of the skull was considered to be isotropic.

The direction of impact is defined as a vector, using a spherical coordinate system centered at the skull's center of mass. Figure 3 illustrates this coordinate system. The azimuthal angle, ϕ, and the polar angle, θ, are provided by the user, which together define a unit direction vector.

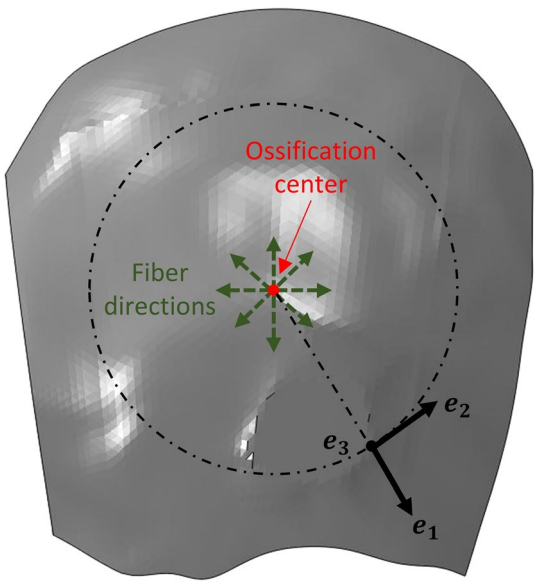

Fig. 2 Cylindrical coordinate system for definition of material orientation

The impact velocity vector is parallel to the impact direction vector. A rigid plate (the impact surface) in the model is then translated and rotated such that it is perpendicular to the velocity vector (i.e., creates a normal impact).

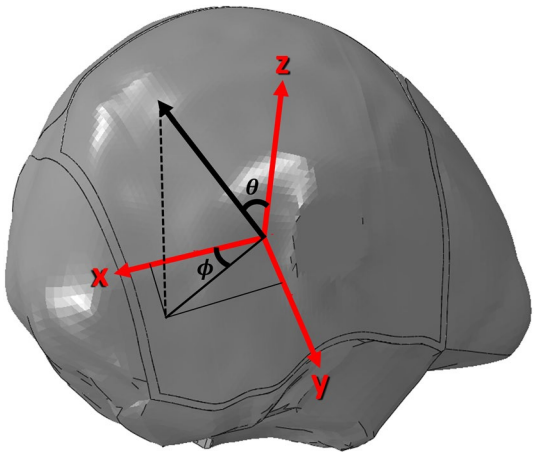

Fig. 3 Definition of the impact direction vector (black arrow) using two angles (ϕ and θ) in the local coordinate system

The magnitude of the initial velocity immediately before impact is calculated from impact height H using:

$$V_{\text{initial}} = \sqrt{2gH}, \tag{1}$$

where g is the local gravitational acceleration.

The Cartesian components of velocity in the Abaqus global coordinate system are computed from the components of the impact direction vector. After all impact parameters are determined, an Abaqus input file is generated. Using this input file, a dynamic simulation of the uncracked model is conducted to extract stress/strain response.

2.3 Initial crack insertion

Based on the criterion proposed by Hajiaghamemar et al. (2018), a crack on the infant skull tends to initiate in the location where the maximum principal stress first exceeds 25 MPa, with a 50% probability. In this work, we adopted the same criterion. The framework inserts a crack at the location where the average maximum principal stress of an element first exceeds 25 MPa. The time instance where the criterion is first exceeded is denoted as t_{initial}.

In this framework, we assume that any initial crack will be oriented such that the equivalent stress intensity factor (K_{Eq}) is maximized. The equivalent stress intensity factor is defined as:

$$K_{\text{Eq}} = \sqrt{K_{\text{I}}^2 + K_{\text{II}}^2 + K_{\text{III}}^2}, \tag{2}$$

where K_{I}, K_{II} and K_{III} denote the Mode I, II and III stress intensity factors, respectively.

To determine the initial crack orientation, a single through-thickness crack of length 2 mm is inserted in the model at five different orientations ($\pm 60°, \pm 30°$ and $0°$) in five independent simulations. An initial crack length of 2 mm is chosen to match the resolution of clinical CT scanners commonly used to identify fractures in bones (Vannier et al. 1984; Jacobsen et al. 2009; Grassberger et al. 2011). Displacements, stresses, and crack-face contact forces at time $t = t_{\text{initial}}$ are extracted to compute all three modes of SIFs for each crack orientation. The orientation that yields the highest average K_{Eq} value along the crack front is considered to be the mechanically preferred orientation of the initial crack. Figure 4 depicts the process of identifying the location of initial crack and the orientations of candidate cracks considered in the framework. Even though Fig. 4 only shows one initiation site, multiple initiation sites at different locations are possible, provided they meet the initiation criterion. The same procedure is applied to each initiation site to determine its preferred orientation.

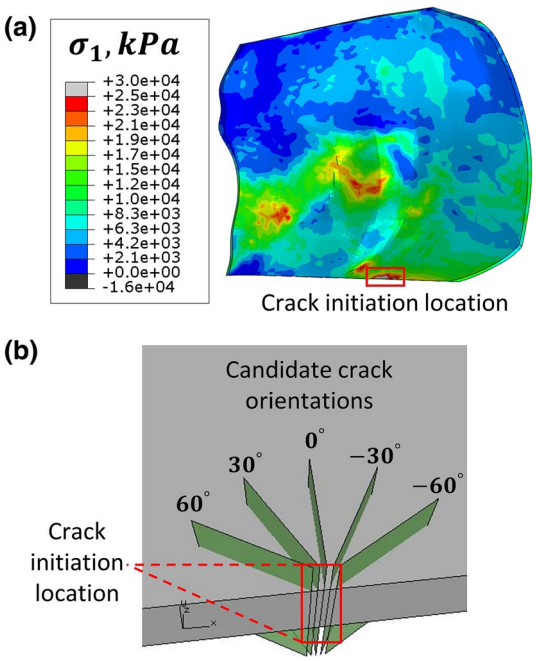

Fig. 4 **a** Example maximum principal stress distribution on the right parietal bone with the crack-initiation site identified (box). The rest of the skull is hidden for visualization. **b** Five candidate crack orientations, depicted simultaneously for visualization

2.4 Calculation of stress intensity factors

In this work, continuous crack growth during impact is approximated by discrete time steps, each of duration 0.1 ms. In time step i, the duration of the impact simulation is $t_{\text{current}} = t_{\text{initial}} + \frac{i}{10}$ ms. SIFs are calculated in each time step for all crack fronts as the crack-growth driving force.

In FRANC3D, the M-integral is the most accurate method for extracting SIFs (Fracture Analysis Consultants 2018), which utilizes a general anisotropic formulation developed

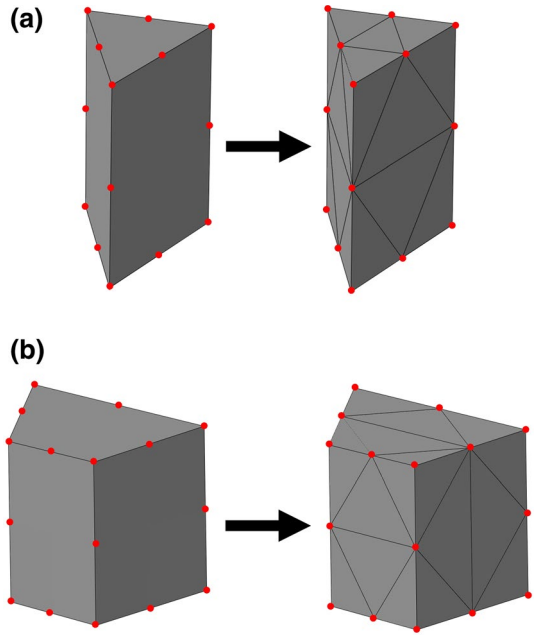

Fig. 5 Partition process on **a** C3D15, **b** C3D20 (nodes shown with red dots) Note that all nodes are retained before and after partition

Table 2 Comparison of averaged SIFs from two methods

Mode	Quadratic template elements (MPa $\sqrt{\text{mm}}$)	Partitioned linear elements (MPa $\sqrt{\text{mm}}$)	Percent difference (%)
K_{I}	10.2	11.0	7.84
K_{II}	− 19.0	− 20.2	6.32
K_{III}	− 7.3	− 7.1	− 2.74

by Warzynek et al. (2005) based on the near-crack stress/strain fields derived by Hoenig (1982). However, structured, quadratic template elements (e.g., quadratic wedge, C3D15, and quadratic hexahedron, C3D20) are needed on the crack front to allow for calculation of *M*-integral in the FRANC3D implementation (v.7.1.1). The above-mentioned element types are not supported in the Abaqus/Explicit (v.6.16) element library. To allow for calculation of the *M*-integral in explicit simulations, an in-house code was built into the framework to modify the mesh prior to the analysis. In this step, each unsupported element is partitioned into multiple linear tetrahedral elements (i.e., C3D4) while preserving all nodes of the original quadratic element. Figure 5 illustrates this partition process on two element types. The effect of partitioning on the accuracy of SIFs was assessed by a case study, the results of which are presented in Table 2. Partitioning inevitably introduces some error, due to the reduction in element quality and loss of quadratic shape functions. The maximum error induced by partitioning was 7.84%, with a mean error of 3.81%, which was considered acceptable for our framework.

Once the partition process is completed, Abaqus/Explicit is used to analyze the modified mesh. FRANC3D leverages displacements and contact forces on the crack-front template nodes to compute SIFs.

2.5 Crack propagation

Crack propagation is dictated by a material's resistance to crack growth (i.e., the material fracture toughness). In bones, crack toughening mechanisms (i.e., crack bridging) lead to an increased fracture toughness with increased crack length (Nalla et al. 2005; Zimmermann et al. 2010). Such behavior is modeled by an increasing *R* curve. In the absence of experimental data for human infant cranial bone, the *R* curve is assumed to take an exponential form. This hypothetical relation is given in Eq. 3:

$$K_{\text{Ic}}(a) = K_{\text{Ic},0}\left(2 - \text{e}^{-0.05a}\right), \tag{3}$$

where $K_{\text{Ic},0}$ and a denote the initial Mode I fracture toughness and the crack length, respectively.

In human cortical bones, crack-growth resistance depends not only on crack length, but also on collagen fiber direction (Nalla et al. 2005; Koester et al. 2008). Because the infant skull contains trabecular fibers that radiate outward from the ossification center, it is reasonable to assume that skull fracture toughness also depends on fiber direction. Pettit (2000) proposed the following empirical relationship that relates fracture toughness in any arbitrary direction to the two principal fracture-toughness values:

$$K_{\text{Ic}}(\beta) = K_{\text{Ic},\parallel}\cos^2\beta + K_{\text{Ic},\perp}\sin^2\beta, \tag{4}$$

where β is the angle between an infinitesimal crack extension and local fiber direction. $K_{\text{Ic},\parallel}$ and $K_{\text{Ic},\perp}$ denote the Mode I fracture toughness parallel and perpendicular to fiber direction, respectively.

For convenience, let:

$$\frac{K_{\text{Ic},\perp}}{K_{\text{Ic},\parallel}} = \lambda. \tag{5}$$

In the proof-of-concept simulations presented in Sect. 3, λ is assumed to be 10 in all simulations. This value is comparable to that observed in human cortical bone specimens by Koester et al. (2008).

Combining Eqs. (3)–(5), we have an expression of the evolution of fracture toughness, or, the *R* curve:

$$K_{\text{Ic}}(\beta, a) = K_{\text{Ic},\parallel,0}\left(2 - \text{e}^{-0.05a}\right)(\cos^2\beta + \lambda\sin^2\beta). \tag{6}$$

From data reported by Bojtár et al. (1994), Mode I fracture toughness of human adult skull is approximately

$23.7 \pm 6.99\,\text{MPa}\sqrt{\text{mm}}$. It is reasonable to assume that infant skulls have lower strength than adult ones. Due to the lack of experimental data on infant skulls, $K_{\text{Ic},\|,0}$ is assumed to be 5 MPa $\sqrt{\text{mm}}$, which is about 21% of that of adult skull.

In this work, the maximum generalized stress criterion (Fracture Analysis Consultants 2018) was adopted to calculate crack kink angle, which is a combination of the maximum tangential stress criterion (Erdogan and Sih 1963) and the maximum shear stress criterion. This criterion was chosen because it accounts for both opening-dominated (Mode I) fracture as well as shear-dominated (Mode II and III) fracture, both being possible due to the complex deformation during impact. For an isotropic material, SIFs of an infinitesimal crack extension at angle $\Delta\alpha$, denoted by k, can be related to SIFs of the main crack as (Pettit et al. 2013):

$$k_{\text{I}}(\Delta\alpha) = \cos\frac{\Delta\alpha}{2}\left(K_{\text{I}}\cos^2\frac{\Delta\alpha}{2} - \frac{3}{2}K_{\text{II}}\sin\Delta\alpha\right), \tag{7}$$

$$k_{\text{II}}(\Delta\alpha) = \frac{1}{2}\cos\frac{\Delta\alpha}{2}(K_{\text{I}}\sin\Delta\alpha + K_{\text{II}}(3\cos\Delta\alpha - 1)), \tag{8}$$

$$k_{\text{III}}(\Delta\alpha) = K_{\text{III}}\cos\frac{\Delta\alpha}{2}. \tag{9}$$

Even though infant skull bones are highly anisotropic, we assume that the above relationships hold. The maximum generalized stress criterion predicts that crack kinks at an angle $\Delta\alpha$ that maximizes the driving force (either opening or shearing). The maximum driving force is defined as:

$$k_{\max}(\Delta\alpha) = \max[k_{\text{I}}(\Delta\alpha), k_s(\Delta\alpha)], \tag{10}$$

where $k_s(\Delta\alpha)$ is defined as:

$$k_s(\Delta\alpha) = \sqrt{[c_2 k_{\text{II}}(\Delta\alpha)]^2 + [c_3 k_{\text{III}}(\Delta\alpha)]^2}. \tag{11}$$

The coefficients c_2 and c_3 in Eq. (11) are user-defined weight factors to tune the contribution of Mode II shearing and Mode III tearing to better match experimental kink-angle observations (Fracture Analysis Consultants 2018). In this work, coefficients c_2 and c_3 are calculated from the relative magnitudes of K_{II} and K_{III}:

$$c_2 = \frac{K_{\text{II}}}{K_{\text{II}} + K_{\text{III}}}, \tag{12}$$

$$c_3 = \frac{K_{\text{III}}}{K_{\text{II}} + K_{\text{III}}}. \tag{13}$$

At the onset of crack propagation, LEFM requires that the local driving force exceeds the local fracture toughness. That is:

$$k_{\max}(\Delta\alpha) \geq \begin{cases} K_{\text{Ic}}(\beta, a), & \text{if } k_{\max}(\Delta\alpha) = k_{\text{I}}(\Delta\alpha), \\ \frac{\sqrt{3}}{2}K_{\text{Ic}}(\beta, a), & \text{if } k_{\max}(\Delta\alpha) = k_s(\Delta\alpha). \end{cases} \tag{14}$$

When driving force is dominated by shear (i.e., $k_{\max}(\Delta\alpha) = k_s(\Delta\alpha)$), Erdogan and Sih (1963) proposed in the maximum tangential stress criterion that K_{IIc} can be estimated as $\frac{\sqrt{3}}{2}K_{\text{Ic}}$, hence the scaling factor in inequality (14). The kink angle $\Delta\alpha$ can now be found by numerically maximizing Eq. (10) while satisfying inequality (14). When the kink angle is found, the crack is advanced in this direction by a uniform amount of 2 mm. Again, this crack extension is selected to be comparable to the resolution of common clinical CT scanners. FRANC3D reads the crack propagation information (viz., new crack front coordinates) and remeshes the model to reflect the new crack geometry. In cases when inequality (14) is not satisfied for any admissible $\Delta\alpha$ between $-90°$ and $90°$, no crack growth will occur in the current load step and the same crack geometry is used in the next analysis step.

2.6 Crack stability

Whenever a crack propagates, crack stability is checked before moving to the next time increment. To do so, the newly formed crack is loaded again to the current time increment, where SIFs are evaluated on the new crack front. If inequality (14) is again satisfied (i.e., crack is predicted to propagate without any increase in load), the crack is considered to be unstable and will be propagated again in the current time increment. This check process is repeated until the crack stops growing in the current time increment. Then, the analysis proceeds to the next time increment where steps described in Sects. 2.4 through 2.6 are repeated until the end of total impact duration. Crack growth is said to be complete either when the end of the total impact duration is reached or when the crack extends across the entire parietal bone of the skull.

2.7 Proof-of-concept simulations

To evaluate the predictability of the framework, three proof-of-concept simulations were performed. In the first proof-of-concept simulation, we simulated a 14.7 cm drop test of a 5-month-old infant head specimen (Case P12M) as described by Loyd (2011). No information on impact angles was provided. To obtain an estimate of the impact conditions, we first identified a potential crack-initiation site based on the experimentally observed fracture pattern provided in the study. Then, through trial and error, we found the impact parameter set that would lead to crack initiation at the estimated location, using our crack-initiation criterion. Using this method, we found that

parameter set [$\phi = 30°, \theta = 0°, H = 14.7$ cm] gives a reasonable crack-initiation location. The mass of the model was scaled uniformly to match that reported by Loyd.

In the second and third proof-of-concept simulations, we simulated two 82 cm drop experiments reported by Weber (1984) involving 2.3-month-old (case A1) and 4-month-old (case A3) infant whole-body specimens, respectively. The mass of the model was scaled to match that reported in each experiment. Similar to Loyd, no impact angle data were provided. We used the same method outlined above to identify potential crack-initiation sites, and found that parameter sets [$\phi = 8°, \theta = 107°, H = 82$ cm] and [$\phi = -40°, \theta = -50°, H = 82$ cm] gave reasonable initiation locations for cases A1 and A3, respectively, based on the hand-drawn fracture patterns provided in the study.

3 Results

3.1 Comparison with Loyd 2011 data

For the first simulation, at an impact height of 14.7 cm, the maximum principal stress did not exceed our threshold of 25 MPa. Because fracture was observed in the experiment, we lowered our stress threshold to 12 MPa for this simulation, which is approximately the 15th percentile of the parietal ultimate stress distribution, according to data reported by Coats (2007). Given the natural variability in the pediatric skull and other factors that could affect fracture initiation (i.e., cadaver handling, freeze/thawing, etc), we consider this decrease to be realistic. This threshold was first exceeded at $t = 0.0026$ s on the anterior edge of the right parietal bone. Starting from this time increment, a total of 60 time steps were simulated using the simulation framework described in Fig. 1. The crack grew 17 times, reaching a final crack length of approximately 37 mm (measured by tracing each crack increment along the mesh outer surface). The crack extended nominally along the direction of trabecular fibers and eventually arrested near the ossification center. The overall kink angle, as measured from the end of the crack to the coronal suture line, is 82.6°. Loyd observed a similar linear fracture nominally along the fiber direction with a reported length of 40 mm and overall kink angle of about 83.18° (measured by our group from the projection drawing). The comparison between the simulated result and Loyd's experimental result is presented in Fig. 6. The figure from Loyd's paper is modified to only show the right parietal bone region. The simulated result shows good agreement with the experiment in terms of both crack length and nominal crack angle.

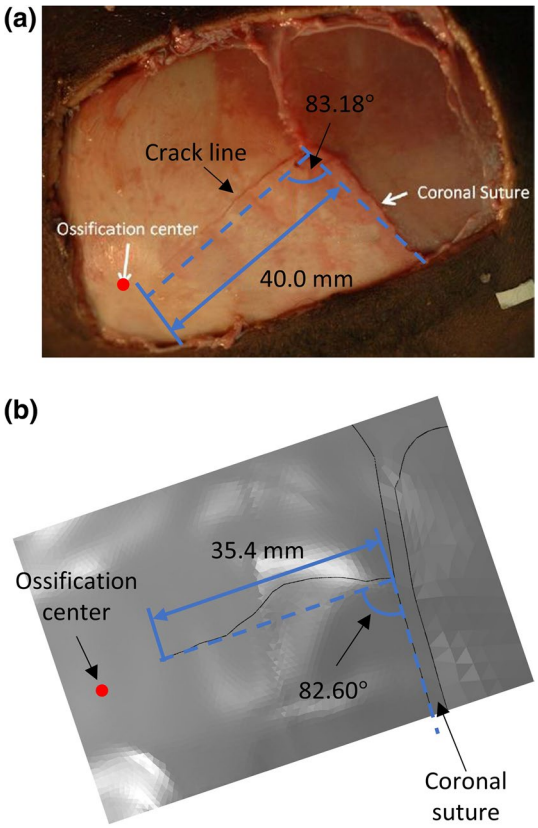

Fig. 6 Comparison with Loyd's experiment, **a** observed crack from experiment [Adapted by permission from Loyd (2011)]. The crack is mostly linear with a tip-to-tail length of 40 mm, **b** simulated result using the computational framework. The simulated crack has a tip-to-tail length of 35.4 mm and actual crack length of 37.0 mm

3.2 Comparison with Weber 1984 data

For simulation of case A1, a crack was predicted to initiate near the ossification center of the right parietal bone. It curved slightly upward and continued to extend nominally along the direction of the trabecular fibers toward the posterior edge of the right parietal bone. In Weber's study, the crack curved upward as it extended away from the posterior edge, similar to our simulation prediction, showing an abrupt kink close to the posterior edge, which is also captured in the simulation; see Fig. 7a, c. The experimentally observed crack from Weber covered about 70% of the right parietal bone length, whereas the simulation prediction covered about 50% of the right parietal bone length. A small crack branch was observed in the experiment. The current framework does not allow for the representation of a branched crack, so it was not captured in the simulation.

For simulation of case A3, two crack-initiation sites were predicted by the framework. One of the cracks initiated on the posterior edge of the right parietal bone, and the other initiated near the ossification center. The two cracks came

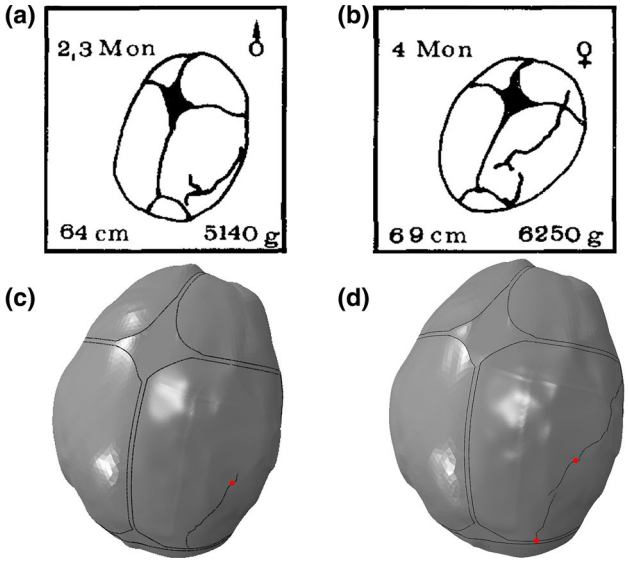

Fig. 7 Weber (1984) experimental results (adapted by permission from Springer Nature: Springer, Zeitschrift fur Rechtsmedizin) and simulated results. **a**, **b** Weber's cadaver experimental fracture patterns from a 82 cm drop of **a** case A1, a 2.3-month-old infant, **b** case A3, a 4-month-old infant onto concrete. **c**, **d** Associated fracture patterns predicted from the computational framework. Crack-initiation sites of the simulations are marked with red dots. In **c**, the framework predicted a shorter crack length as compared to **a**, but the general trend is in agreement. In **d**, the framework predicted two separate cracks, which is in agreement with the Weber drawings in **b**. However, the anterior crack terminated in the inferior region of the bone rather than crossing over the coronal suture

close to coalescing but were manually arrested because coalesced cracks are not possible to mesh in the current framework. The two cracks remain nominally parallel to the superior edge of the right parietal bone until the center crack approached the anterior edge of the right parietal bone, where it extended downward to the anterior inferior corner of the bone. Two nearly coalescing cracks were observed in the experimental drawing as well; see Fig. 7b, d. However, in Weber's study, the posterior side of the center crack first kinked upward then turned flat before branching, which is not captured in the simulation. The anterior side of the center crack continued to extend in a direction parallel to the superior edge of the right parietal bone and extended to the coronal suture. A small crack branch was observed for the center crack. Neither the extension into the frontal bone nor the crack branching was captured in the simulation, as those features are not currently supported.

4 Discussion

In this work, we developed the first computational framework for predicting infant skull fracture based on linear elastic fracture mechanics using adaptive-remeshing technique. Four aspects of this framework deserve further discussion: (1) framework performance, (2) FE model and constitutive relations, (3) assumptions made in the framework and (4) potential applications.

In the three proof-of-concept simulations, the framework predicted similar crack patterns given user-estimated crack-initiation sites and impact conditions. Crack growth along trabecular fiber directions is clearly favored. This is likely a result of the anisotropic fracture-toughness model employed in the framework. This behavior is in agreement with the experimental observations. The predicted crack lengths show different levels of agreement among the three simulations. It predicted very similar length for the Loyd's case P12M and Weber's case A3 while under-predicted the length for Weber's case A1. For case A1, this under prediction is likely due to the overly high fracture toughness and its evolution curve (R curve), as well as to the uncertainty in the exact impact parameters and skull geometry, which were not reported in the experimental study. The similarity between simulation and experiment results is expected to improve if the impact parameters, skull geometries, and material properties were known and accounted for in the model.

Prior to this work, many researchers explored prediction of skull fracture via element deletion methods (Raul et al. 2006; Roth et al. 2010; Li et al. 2019). In element deletion methods, the size and shape of the finite elements dictate the spatial resolution of the predicted crack pattern. In early works that used relatively coarse mesh (Raul et al. 2006) or used hexahedral elements (Roth et al. 2010), unrealistic patchy and disconnected fracture patterns or zig-zagged fracture patterns were predicted. With the use of a refined mesh, Li et al. (2019) predicted smooth crack patterns, but the framework only predicted some of the many crack-initiation sites and had some deviation from the experimental crack paths. In addition, the anisotropic fracture properties of infant skull were not incorporated in any of the previous element deletion models. The inclusion of fracture-toughness anisotropy in our model allows the model to better capture crack growth nominally along trabecular fiber directions, as demonstrated in the proof-of-concept simulations.

It is important to highlight that the implementation of the current framework is independent of the FE model and material properties. This framework can be coupled with a case-specific FE model and material properties to produce case-specific predictions, as opposed to using the same model for different cases. The framework also leaves freedom for the researcher to tune fracture parameters of the model (e.g., mixed-mode weight factors, R curve equation) to better match experimental observations. Although the maximum generalized stress criterion is used for calculating kink angle in the current framework, this choice is somewhat arbitrary. Some researchers suggest that the maximum tangential stress criterion better describes experimental results (Nalla et al.

2005; Hazenberg et al. 2006; Koester et al. 2008), while others suggest the use of the maximum strain energy release rate criterion (Zimmermann et al. 2010). However, there is not a definitive consensus on which one is better. Any of these kink-angle models can be explored by the user without loss of generality.

Many assumptions and simplifications were employed in this framework. We set 2 mm as the length of the initial crack as well as the uniform extension increment of the crack front. Further, a crack was assumed to propagate along a single kink angle and with uniform extension along the three-dimensional crack front. Neither of these assumptions occurs in real life, but were necessary simplifications to balance accuracy, meshability, and computational efficiency. Non-uniform crack growth with individual kink angles for all crack front nodes is possible, but is typically applied to simplified geometries. Creating a complex crack front in an already complex geometry, all while maintaining a structured crack-front template mesh (Warzynek et al. 2005), would be inherently challenging. Increasing complexity in these features can be explored in future refinements of the framework. It is also worth noting that the relationships in Eqs. (7)–(9) are for isotropic materials. They were assumed to hold even for the anisotropic skull in this work. It is unknown whether this is a reasonable assumption. Future experimental efforts are needed to help elucidate the implications of this assumption.

Regardless of these assumptions, the three proof-of-concept simulations bore striking similarities to their experimental counterparts. The general paths and lengths of the fracture patterns were in agreement. Limitations of the framework prevented finer details such as crack branching, and we hope to explore solutions for these aspects in the future. However, in its current state, the framework provides a reasonable approximation of the primary fracture pattern and will be extremely useful in parametric simulations investigating the effects of impact energy and directionality. Further, from the case studies, we determined that the anisotropic fracture toughness of human infant cranial bone is critical to accurate predictions of crack patterns. To date, no one has considered anisotropic fracture-toughness properties in human cranial bone because adult cortical cranial bone is fairly isotropic. This highlights the importance of developing experiments and models specific to infants and children, rather than simply scaling data and models developed for adults.

In summary, this new framework provides a tool to study impact-induced fracture of infant skulls from a computational perspective. We plan to use this tool to parametrically evaluate the effects of impact energy, directionality, and skull geometry on predictions of skull fracture patterns in infants. These data will be critical to understanding the effect and sensitivity of environmental variables on predictions of skull fracture in infants. While the framework is currently used to predict skull fracture patterns given impact height and direction, our hope is to use the model to develop correlations between impact inputs and pattern outputs, such that the inverse approach may be used. Specifically, the ultimate goal is to simulate real-world infant skull injury cases given the impact conditions and material properties to predict whether skull fracture will occur for a case and, if so, what kinds of fracture can be expected. This can ultimately be used in the criminal justice system to assess—from a fundamental mechanics-based approach—the cause of observed fracture in human infant skulls. Furthermore, while this work focuses on infant skull fracture, the fracture simulation framework is general enough that it could be applied to adults, upon modifying the geometry and material properties.

5 Conclusion

This work presents the development, implementation and validation of an innovative finite-element-based framework for simulating high-fidelity crack propagation during impact loading scenarios. The framework utilizes an adaptive-remeshing technique to create a geometrically explicit representation of the crack. Stress intensity factors are calculated as crack-growth driving force to determine onset of crack propagation. Kink angles are calculated following principles of linear elastic fracture mechanics. Fracture-toughness anisotropy of human infant skull is modeled by considering its dependence on direction and crack length. Crack stability is also checked each time a crack propagates.

Three proof-of-concept simulations are presented to demonstrate the capability of the current framework. When compared to experiments, the simulated results predict similar crack lengths and nominal crack-extension directions, which provide confidence in the capability of the modeling framework. The fracture parameters used in the model need to be further calibrated with experimental data. Once complete, this framework can be used to evaluate the effect and sensitivity of environmental variables on predictions of skull fracture, improve design criteria for pediatric safety equipment, and provide objective data to improve the accurate detection of child abuse.

Acknowledgements This project was supported by Award No. 2016-DN-BX-0160, awarded by the National Institute of Justice, Office of Justice Programs, US Department of Justice. The opinions, findings, and conclusions or recommendations expressed in this publication, program, exhibition are those of the authors and do not necessarily reflect those of the Department of Justice. Initial development of the infant skull model was supported by the Centers for Disease Control and Prevention Grant NCIPC R49CE000411. The authors gratefully acknowledge Dr. Bruce Carter for his technical support on issues regarding the use of FRANC3D.

Compliance with ethical standards

Conflict of interest The authors declare that they have no conflict of interest.

References

Asgharpour Z, Baumgartner D, Willinger R, Graw M, Peldschus S (2014) The validation and application of a finite element human head model for frontal skull fracture analysis. J Mech Behav Biomed Mater 33:16–23

Bojtár I, Gálos M, Scharle A (1994) Fracture mechanical analysis of human skull. Period Polytech Civ Eng 38(4):367–374

Chin PL (2011) Stress analysis, crack propagation and stress intensity factor computation of a Ti–6Al–4V aerospace bracket using ANSYS and FRANC3D. Sc Degree Rensselaer Polytechnic Institute Hartford Connecticut

Coats B (2007) Mechanics of head impact in infants. PhD thesis, University of Pennsylvania

Coats B, Margulies SS (2006) Material properties of human infant skull and suture at high rates. J Neurotrauma 23(8):1222–1232

Coats B, Ji S, Margulies SS (2007) Parametric study of head impact in the infant. Technical report, SAE technical paper

Corbani S, Castro J, Miranda A, Martha L, Carter B, Ingraffea A (2018) Crack shape evolution under bending-induced partial closure. Eng Fract Mech 188:493–508

Cunningham C, Scheuer L, Black S (2016) Developmental juvenile osteology. Academic Press, Berlin

Davis B, Wawrzynek P, Ingraffea A (2014) 3-D simulation of arbitrary crack growth using an energy-based formulation—part I: planar growth. Eng Fract Mech 115:204–220

Erdogan F, Sih G (1963) On the crack extension in plates under plane loading and transverse shear. J Basic Eng 85(4):519–525

Farley R, Reece R, Robert M (2002) Recognizing when a child's injury or illness is caused by abuse. US Department of Justice, Office of Juvenile Justice and Delinquency Prevention, NCJ 160938

Fracture Analysis Consultants, Inc. (2018) FRANC3D reference manual, version 7.2 (online). http://www.fracanalysis.com/software.html. Accessed 16 Feb 2019

Grassberger M, Gehl A, Püschel K, Turk E (2011) 3D reconstruction of emergency cranial computed tomography scans as a tool in clinical forensic radiology after survived blunt head trauma—report of two cases. Forensic Sci Int 207(1–3):e19–e23

Hajiaghamemar M, Lan IS, Christian CW, Coats B, Margulies SS (2018) Infant skull fracture risk for low height falls. Int J Leg Med 133:1–16

Hazenberg JG, Taylor D, Lee TC (2006) Mechanisms of short crack growth at constant stress in bone. Biomaterials 27(9):2114–2122

Hoenig A (1982) Near-tip behavior of a crack in a plane anisotropic elastic body. Eng Fract Mech 16(3):393–403

Jacobsen C, Bech BH, Lynnerup N (2009) A comparative study of cranial, blunt trauma fractures as seen at medicolegal autopsy and by computed tomography. BMC Med Imaging 9(1):18

Koester KJ, Ager Iii J, Ritchie R (2008) The true toughness of human cortical bone measured with realistically short cracks. Nat Mater 7(8):672

Lee H, Choi J, Jung K, Im YT (2009) Application of element deletion method for numerical analyses of cracking. J Achiev Mater Manuf Eng 35(2):154–161

Leventhal JM, Thomas SA, Rosenfield NS, Markowitz RI (1993) Fractures in young children: distinguishing child abuse from unintentional injuries. Am J Dis Child 147(1):87–92

Li Z, Luo X, Zhang J (2013) Development/global validation of a 6-month-old pediatric head finite element model and application in investigation of drop-induced infant head injury. Comput Methods Programs Biomed 112(3):309–319

Li Z, Liu W, Zhang J, Hu J (2015) Prediction of skull fracture risk for children 0–9 months old through validated parametric finite element model and cadaver test reconstruction. Int J Leg Med 129(5):1055–1066

Li X, Sandler H, Kleiven S (2019) Infant skull fractures: Accident or abuse? Evidences from biomechanical analysis using finite element head models. Forensic Sci Int 294:173–182

Loyd AM (2011) Studies of the human head from neonate to adult: an inertial, geometrical and structural analysis with comparisons to the ATD head. Duke University, Duke

Lynn PP, Ingraffea AR (1978) Transition elements to be used with quarter-point crack-tip elements. Int J Numer Methods Eng 12(6):1031–1036

Metcalf RM, Comstock JM, Coats B (2019) High-rate anisotropic and region-dependent properties in human infant cranial bone. Summer biomechanics, bioengineering, and biotransport conference. Seven Springs, PA June 2019

Nalla R, Stölken J, Kinney J, Ritchie R (2005) Fracture in human cortical bone: local fracture criteria and toughening mechanisms. J Biomech 38(7):1517–1525

Nguyen O, Repetto E, Ortiz M, Radovitzky R (2001) A cohesive model of fatigue crack growth. Int J Fract 110(4):351–369

Peterson J, Dechow PC (2002) Material properties of the inner and outer cortical tables of the human parietal bone. Anat Rec 268(1):7–15

Pettit RG (2000) Crack turning in integrally stiffened aircraft structures. PhD thesis, Cornell University

Pettit R, Annigeri B, Owen W, Wawrzynek P (2013) Next generation 3D mixed mode fracture propagation theory including HCF–LCF interaction. Eng Fract Mech 102:1–14

Raul JS, Baumgartner D, Willinger R, Ludes B (2006) Finite element modelling of human head injuries caused by a fall. Int J Leg Med 120(4):212–218

Roth S, Raul JS, Willinger R (2008) Biofidelic child head FE model to simulate real world trauma. Comput Methods Programs Biomed 90(3):262–274

Roth S, Raul JS, Willinger R (2010) Finite element modelling of paediatric head impact: global validation against experimental data. Comput Methods Programs Biomed 99(1):25–33

Sahoo D, Deck C, Yoganandan N, Willinger R (2013) Anisotropic composite human skull model and skull fracture validation against temporo-parietal skull fracture. J Mech Behav Biomed Mater 28:340–353

Shih C, Lorenzi Hd, German M (1976) Crack extension modeling with singular quadratic isoparametric elements. Int J Fract 12(4):647–651

Song JH, Areias PM, Belytschko T (2006) A method for dynamic crack and shear band propagation with phantom nodes. Int J Numer Methods Eng 67(6):868–893

Spear AD, Priest AR, Veilleux MG, Ingraffea AR, Hochhalter JD (2011) Surrogate modeling of high-fidelity fracture simulations for real-time residual strength predictions. AIAA J 49(12):2770–2782

US Department of Health & Human Services, Administration for Children and Families, Administration on Children, Youth and Families, Children's Bureau (2019) Child maltreatment 2017 (online). https://www.acf.hhs.gov/cb/research-data-technology/statistics-research/child-maltreatment. Accessed 8 Aug 2019

Vannier MW, Marsh JL, Warren JO (1984) Three dimensional CT reconstruction images for craniofacial surgical planning and evaluation. Radiology 150(1):179–184

Warzynek PA, Carter BJ, Banks-Sills L (2005) The M-integral for computing stress intensity factors in generally anisotropic materials. Technical report, NASA/CR–2005–214006

Wawrzynek P, Carter B, Hwang CY, Ingraffea A (2010) Advances in simulation of arbitrary 3D crack growth using FRANC3DV5. J Comput Struct Eng Inst Korea 23(6):607–613

Weber W (1984) Experimental studies of skull fractures in infants. Z Rechtsmed J Leg Med 92(2):87–94

Weber W (1985) Biomechanical fragility of the infant skull. Z Rechtsmed J Leg Med 94(2):93–101

Zhang L, Yang KH, Dwarampudi R, Omori K, Li T, Chang K, Hardy WN, Khalil TB, King AI (2001) Recent advances in brain injury research: a new human head model development and validation. Technical report, SAE technical paper

Zimmermann EA, Launey ME, Ritchie RO (2010) The significance of crack-resistance curves to the mixed-mode fracture toughness of human cortical bone. Biomaterials 31(20):5297–5305